Supplementary Information:

Quantitative, time-resolved measurement of membrane protein-ligand interactions using microcantilever array sensors

Thomas Braun, Murali Krishna Ghatkesar, Natalija Backmann, Wilfried Grange, Pascale Boulanger, Lucienne Letellier, Hans-Peter Lang, Alex Bietsch, Christoph Gerber and Martin Hegner*

* Corresponding author: Prof. Martin Hegner, CRANN, School of Physics, Trinity College Dublin, Ireland; martin.hegner@tcd.ie

Workflow of the experimental steps needed for the described experiments

A short guide through the complete experimental procedure is presented in **Figure Suppl. 1**. Additionally, more specific information can be found in the manuscript. The FhuA gene was cloned into *E. coli* for over-expression with an engineered His-tag for affinity purification as described before [1] (**panel a**). The membranes were harvested after cell-rupture and were solubilized with the detergent n-octyl-β-D-glucopyranoside [1] (**panel b**). The solubilized FhuA protein was purified on an affinity Ni-NTA-column [2] (**panel c**). The purified protein was reconstituted in liposomes by mixing it with solubilized lipids and subsequent removal of the detergent by dialysis [3,4] (**panel d**). Depending of the protein/lipid ratio, the protein was reconstituted as a highly ordered protein array (2D-crystal) or as vesicles (**panel e**, compare with **Fig. 1** of manuscript). To immobilize the proteoliposomes on the cantilever, ink-jet spotting technology combined with a humidity chamber was used (**panel f**, compare with **Fig. 2** and **3** of manuscript). The functionalized cantilever was mounted in the measurement chamber and a solution containing T5-phages was injected. The T5 production was described previously [5]. The frequency response (amplitude and phase) was constantly monitored by a laser detection read-out (**panel g**). These spectra were post-processed using the NOSE-tool software package [6, 7, 8] to obtain the mass adsorption during the experiment (**panel h**, see **Fig. 4** of manuscript).

© 2009 **Macmillan Publishers Limited. All rights reserved.**

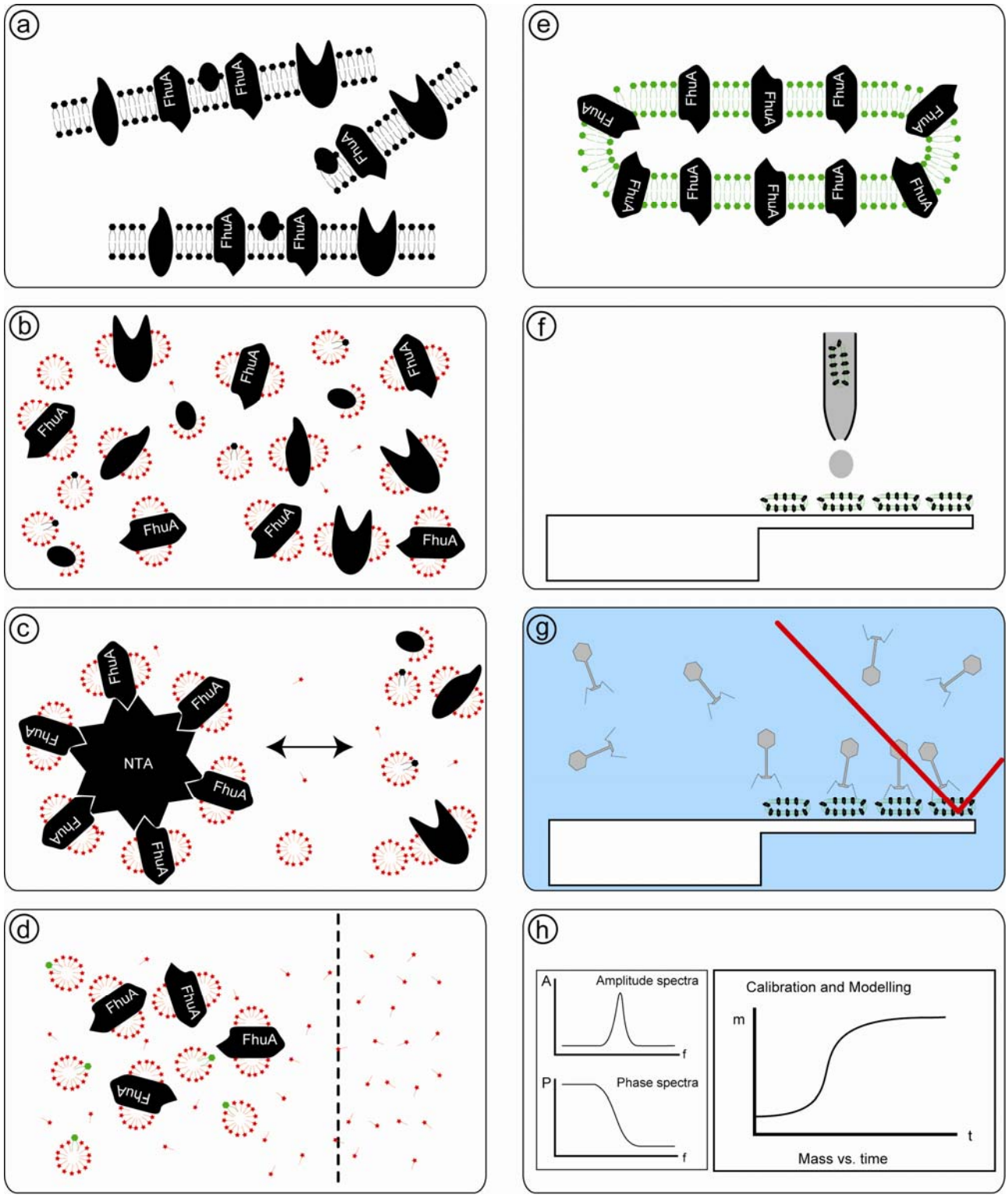

Figure Suppl. 1: Overview over major experimental steps. a): Protein expression of FhuA. b): Solubilization of membranes with detergent (red). c): Affinity purification with an NTA-column. d): Reconstitution of the solubilized FhuA protein in lipid-vesicles by dialysis (green: added lipid). e): Proteoliposome of FhuA vesicles. f): Ink-jet spotting of FhuA proteoiposomes on the upper cantilever interface. g): Phage binding experiment by dynamic mode cantilever sensor. h): Post-processing of recorded spectra (raw-data) to obtain mass changes during experiment.

© 2009 **Macmillan Publishers Limited. All rights reserved.**

Theory of the data evaluation

A more detailed discussion about the theory can be found in ref. [6], and a description about the NOSEtools software used for data processing is given in ref. [7].

The vibration dynamics of a cantilever in vacuum are characterized by the equation of motion, which is given by

$$\underbrace{EI\frac{\partial^4 u(x,t)}{\partial x^4}}_{\text{restoring force}} + \underbrace{C_0\frac{\partial u(x,t)}{\partial t}}_{\text{intrinsic damping}} + \underbrace{\frac{m_c}{L}\frac{\partial^2 u(x,t)}{\partial t^2}}_{\text{inertial force}} = 0 \qquad (1)$$

EI is the flexural rigidity of the cantilever spring. *E* is the Young's modulus and *I* the moment of inertia. C_0 is the intrinsic damping coefficient per unit length that describes internal losses; m_c is the mass of the cantilever and *L* the length of the cantilever. *U(x; t)* is the detection of the cantilever perpendicular to the cantilever axis. *X* is the coordinate along the cantilever axis and *t* is time.

For cantilevers vibrating in a liquid environment and driven by a piezoelectric crystal plate, three additional forces have to be taken into account: First, the motion of the cantilever experiences an additional resistance, because not only the cantilever, but also a specific amount of the fluid has to be accelerated. This means that the surrounding fluid acts on the cantilever as if an additional mass m_l is attached to the cantilever. This commoving mass is also called 'virtual mass'. Second, an additional dissipative force per unit length acts on the cantilever that is proportional to the velocity, $g_v = -C_v\frac{\partial u(x,t)}{\partial t}$, where C_v is the external dissipation coefficient. Third, an external periodic force per unit length acts on the cantilever (F(x; t)). Taking these three additional forces into account, Eq. (1) can be expanded to

$$EI\frac{\partial^4 u(x,t)}{\partial x^4} + \underbrace{C_v\frac{\partial u(x,t)}{\partial t}}_{\text{external damping}} + C_0\frac{\partial u(x,t)}{\partial t} + \underbrace{\frac{m_l}{L}\frac{\partial^2 u(x,t)}{\partial t^2}}_{\text{inertial force of "virtual mass"}} + \frac{m_c}{L}\frac{\partial^2 u(x,t)}{\partial t^2} = \underbrace{F(x,t)}_{\text{periodic driving force}} \qquad (2)$$

© 2009 **Macmillan Publishers Limited. All rights reserved.**

In this study we detect an uptake of tiny amounts of mass distributed over the entire cantilever that is due to ligand-receptor interaction on the cantilever surface. Therefore, this additional mass must be taken into account in all formulas above for the total mass:

$$m_{\text{total}} = m_c + m_l + \underbrace{\Delta m}_{\text{mass load}} \tag{3}$$

Equation 2 can be solved for a rectangular cantilever with evenly distributed mass load to describe the recorded frequency spectra for the amplitude and phase. The eigenfrequency f_{0n} of the cantilever in mode *n* is given as follows:

$$f_{0n} = \frac{\alpha_n^2}{2\pi}\sqrt{\frac{k}{3(m_{tot})}} \tag{4}$$

k is the cantilever constant ($k = 3EI/L^3$). The α_n are related to the different eigenvalues of the harmonics and are fixed by the boundary conditions [9]. ($\alpha_1 = 1.875$, $\alpha_2 = 4.694$, $\alpha_3 = 7.854$, $\alpha_4 = 11.0$, $\alpha_{5\ldots n} = \pi(n-0.5)$.)

The amplitude of the response of the n_{th} harmonics in dependence of the frequency of the driving force *f* is given according to the model of a damped harmonic oscillator by

$$u_n(f) = \frac{u_{\max} f_{0n}^2}{\sqrt{(f_{0n}^2 - f^2)^2 + \frac{\gamma^2 f^2}{\pi^2}}} \tag{5}$$

The damping factor γ is defined by

$$\gamma = \frac{C_0 + C_v}{\frac{2}{L} m_{tot}} \tag{6}$$

In our case the damping factor is dominated by the liquid .

The function 5 is also called resonance curve and has a maximum at the peak-frequency

$$f_n = \sqrt{f_{0n}^2 - \frac{\gamma^2}{2\pi}} \tag{7}$$

© 2009 **Macmillan Publishers Limited. All rights reserved.**

The phase between response and driving force in dependence of the frequency of the driving force is given by:

$$\varphi(f) = \arctan \frac{-\gamma f}{\pi(f_{0n}^2 - f^2)} \qquad (8)$$

The eigenfrequency f_{0n} is defined as the point where the phase curve has its steepest slope. For the phase spectra, the damping γ only affects the slope around the eigenfrequency but not the position in the spectra. In contrast to that, the amplitude peak gets broader (lower Q factor) and the peak-frequency is shifted towards lower values. Note that the external damping dominates the system in liquid [6].

In order to determine the mass load Δm, the virtual mass m_l must be determined at the beginning of the experiment (calibration). The external damping C_v is always defined by the amplitude peak width and the peak-frequency or by the gradient around the phase turn-point respectively.

Experimental data analysis

As mentioned in the **Materials and Methods** section, the total mass was estimated from a fit of the amplitude *versus* frequency spectra (Eq. 5) (**Figure Suppl. 2**). The relation between the total mass and the eigenfrequency (damping coefficient) was given by Eq. 4 (Eq. 6). The 'virtual mass' as well as the mass of the cantilever were calibrated at the beginning of the measurement and then was kept constant over the experiments [10, 8]. For the experiment presented in the manuscript, only one peak of the amplitude spectrum was fitted.

© 2009 **Macmillan Publishers Limited. All rights reserved.**

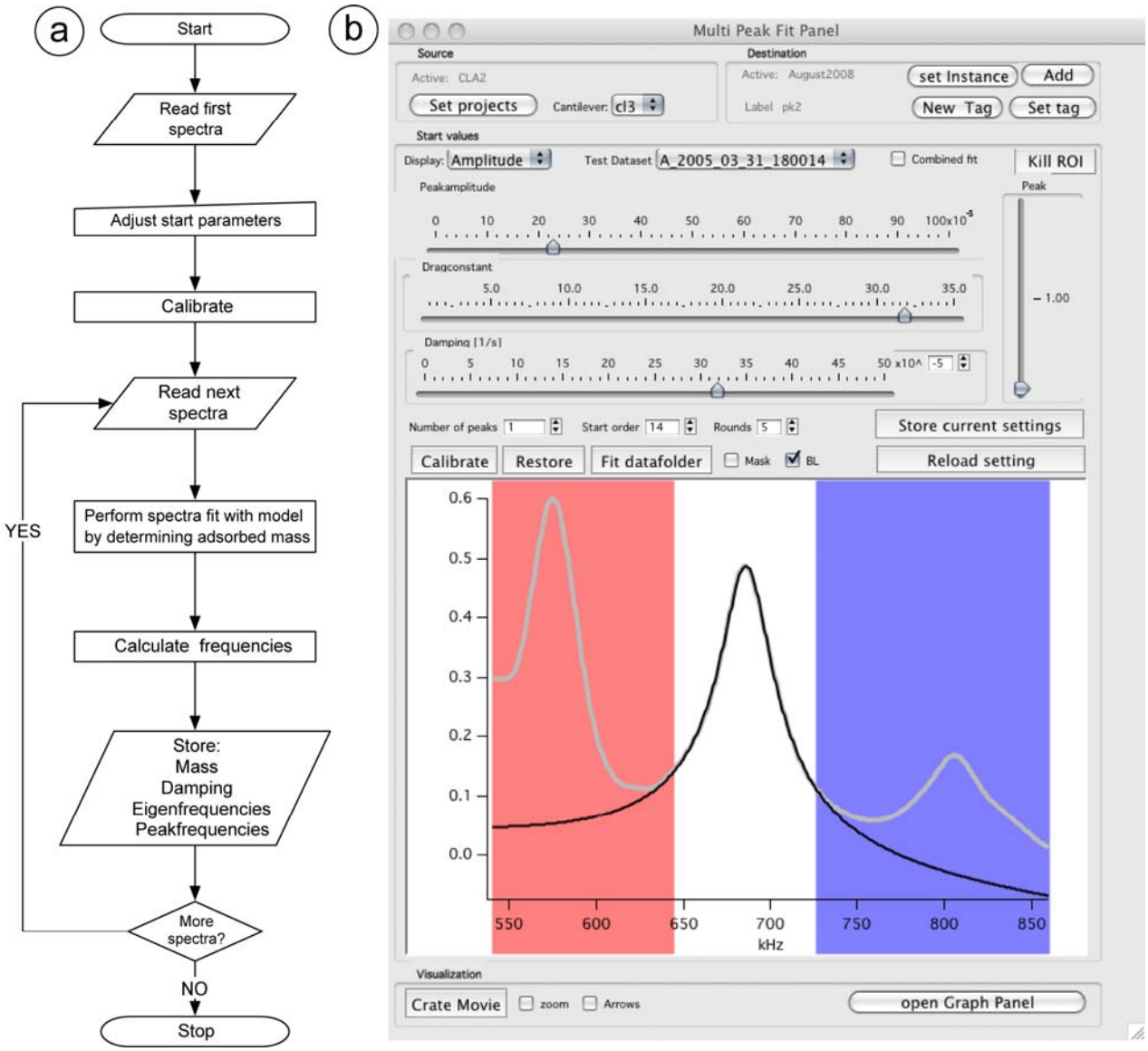

Figure Suppl. 2: Simplified flow diagram for peak tracking and model fit algorithms. a) Work flow for mass determination by modelling a series of spectra. b) Graphical user interface for data modelling. Note the preview-window with the raw data (thick grey line) and the model fit in black.

In situ reference cantilevers

When planning differential nano-mechanical cantilever array experiments, the choice of the reference cantilever functionalization is certainly one of the most crucial issues. For measurements involving the binding of T5 on FhuA receptors, cantilevers coated with casein only were found to be ideal negative controls (see also **figure suppl. 5**) due to the absence of non-specific binding on the positive control cantilevers (FhuA coated) when the FhuA is inactivated (**figure 1f and figure suppl. 3a**). The situation might be different when also non-specific interactions on the positive control cantilevers are likely to occur.

© 2009 **Macmillan Publishers Limited. All rights reserved.**

To illustrate this behavior, we have performed nano-mechanical experiments involving the binding of ferrichrome (MW 687.7 Da), an iron-chelating molecule, which allows the translocation of iron across FhuA channels[11]. **Figure suppl. 3c** shows the result of a binding experiment of the small ligand ferrichrome to FhuA functionalized membrane protein cantilevers. Here, similar positive and negative control cantilevers as for experiments involving T5 where used. Considering the number of active and accessible FhuA sites on the cantilevers ($5.3X10^8$), the expected mass uptake is smaller than 1 pg, much smaller than our current detection of limit of our apparatus (~ 0.5 ng). After recording the baseline in buffer, ferrichrome was injected at a concentration of 1 µM, slightly above its dissociation constant [12]. While the casein reference cantilever does not shown a mass uptake during the injection of ferrichrome [600µl of a [1µM] solution (10 µl/min)], the positive control cantilever (membrane-FhuA functionalized) evidence for a mass uptake of about 2 ng (**figure suppl. 3c**). This non-specific binding (found to be reproducible for three independent measurements performed on different arrays) is attributed to electrostatic interactions between the lipid head groups and the negatively charged ferrichrome molecules (**figure suppl. 3b**). In summary it remains a major challenge for surface based techniques (cantilevers, surface plasmon resonance [13], quarz crystal microbalance [14] (QCM)) to elucidate specific binding kinetics of small ligands.

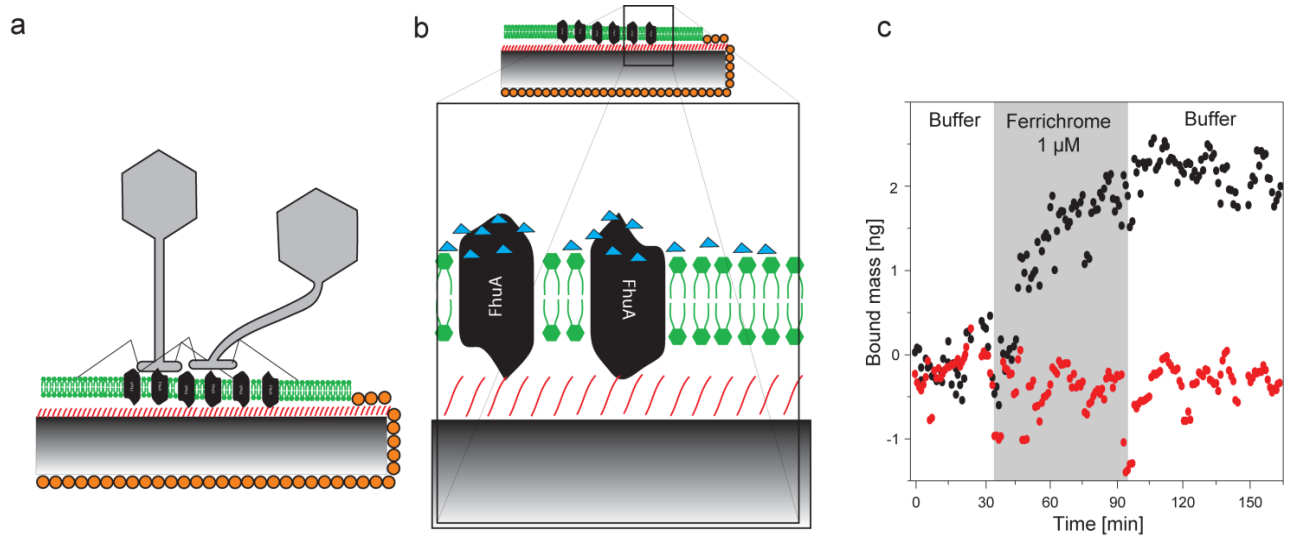

Figure Suppl. 3: Ligand binding on native membrane protein functionalized microcantilever. T5 virus (grey hexagonal structures), lipid bilayer (green), FhuA trans-membrane protein (black), self-assembled hetero-bifunctional monolayer (red), Cantilever (black-grey, not drawn to scale), casein (orange), ferrichrome (blue triangle). a) Specific binding of T5 virus to FhuA membrane protein. No binding is observed on casein protected interfaces nor on lipid area depleted from FhuA (or having non-active FhuA receptors, **figure 1f**). b) Binding of ferrichrome to the FhuA membrane proteins and the lipid bilayer. No binding is observed on casein protected interfaces but non-specific interactions occur between ferrichrome and the lipid bilayer.

© 2009 **Macmillan Publishers Limited. All rights reserved.**

c) Binding of ferrichrome to FhuA membrane protein functionalized sensor (black dots), casein blocked reference cantilever (red dots).

Phage load of FhuA containing vesicles

The long tail of T5 provides an ample flexibility between the anchoring point of the phage and the DNA containing head as demonstrated by the following image (see also **fig. suppl. 3a**). The binding experiment was performed as described above in the presence of 100 nM ferrichrome.

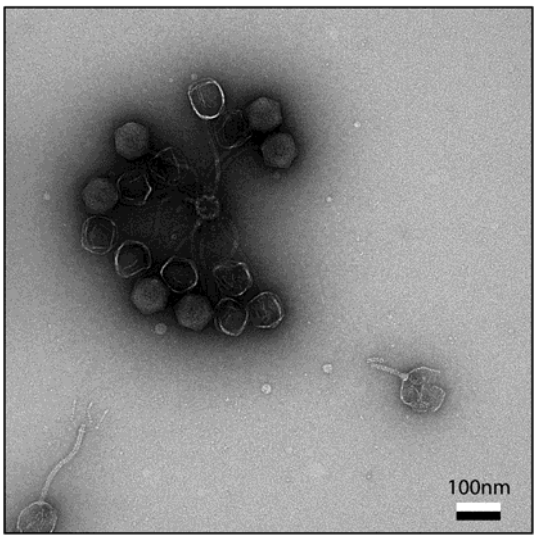

Figure Suppl. 4: TEM image of T5 virus binding to a small proteoliposome which was pre-incubated with 100 nM ferrichrome. The small proteoliposome in the middle is surrounded by T5 phage particles.

Cantilever functionalization

Throughout the functionalization process, the variability of the FhuA protein (receptor) density was minimized. As such, the binding experiments presented in the manuscript (**Figure 5**) show a good repeatability. We mention, however, both the preparation of the reconstituted FhuA membrane receptors and the functionalization of sensing cantilevers is a demanding task.

The FhuA must be reconstituted in proteoliposomes due to the nature of the amphiphilic membrane protein. We used a flow-controlled machine originally developed for 2D crystallization [3]. One assay contained maximally 50 µl as start volume; however, due to loss of material and osmetic/flow pressure effects only 30 µl are recovered at the end. Since in every protein purification the amount of associated lipids with the protein varies, we performed the reconstitution preparations always with a series of different lipid-protein ratio. Therefore, only a limited amount of experiments can be performed with one sample. Densely packed to mosaic crystalline vesicles gave good results with phage binding, whereas high crystalline sheets did not show activity if adsorbed on cantilever surfaces. The application of an ink-jet spotting device (using pico-liter droplets as shown in **Figure**

© 2009 **Macmillan Publishers Limited. All rights reserved.**

2 of the manuscript) is still enabling many experiments with one batch and reduces the amount of material used for the functionalization. Note, however, that a standard micro-capillary functionalization procedure can be used for other experiments (genomics, soluble proteins) [15, 16].

Specificity of binding and blocking of unspecific binding by casein

We examined also the underside of the ink-jet functionalized cantilevers by tapping mode AFM (as in **Figure 3** of manuscript). Only a very small amount of proteoliposomes structures were observed, most probably from the first washing step after functionalization with the ink-jet spotter, which selectively wets the upper cantilever surface with the proteoliposome solution. This is in good agreement with bacteriorhodopsin experiments performed previously [17]. We also made control experiments for unspecific phage adsorption on the cantilever backside and could only find few phage particles (maximally 1 to 2 phage head/μm^2, **figure suppl. 5**). However, casein could form inhomogeneous micellular structures which grow with time [18] and might look very similar to T5 Phages in the AFM [19] which could complicate the interpretation but none were found when fresh casein was used.

The cantilever was functionalized as described in the manuscript and the array was incubated for 1.5h in a solution containing 20mM Tris HCL pH 8, 5mM $MgCl_2$, 5mM $CaCl_2$, 100mM NaCl, 0.01% NaN_3 and 0.2pM PFU of T5 phages. Arrows indicate regions which could be interpreted as adsorbed virus particles.

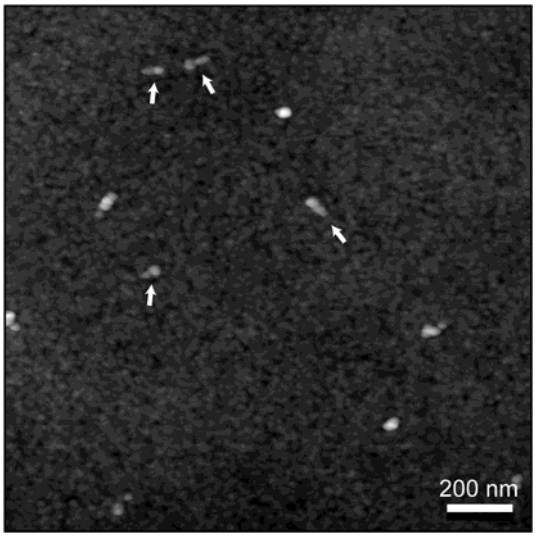

Figure Suppl. 5: AFM image of the backside of cantilevers passivated with casein and incubated for 1.5h in a solution of 0.5pM T5 solution (arrows mark either T5 phages or possible casein aggregates) Note that the conditions here are different from the in-situ experiments presented in the manuscript.

© 2009 **Macmillan Publishers Limited. All rights reserved.**

We performed EM experiments with casein which could form micelles when stored over time and negative stain similar to the EM pictures performed in **figure 1** of the manuscript. However, the surface structure and charge are different than the situation *in situ* on the cantilever.

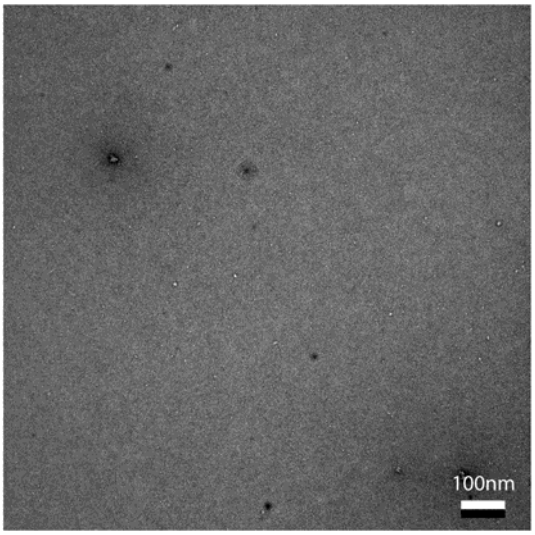

Figure Suppl. 6: Casein adsorbed on glow-discharged EM grid in negative stain (protein white). A fresh solution of nominal 1mg/ml casein (filtered with 0.2µm filter) was incubated for 1 min on a 20s glow discharged EM carbon-palladium grid and stained for 2x12sec with 2% Uranyl acetate.

The estimated density of unspecific T5 particles is around 1 to 2 particles/μm^2. We would like to point out, that viruses must avoid unspecific binding to be successful in nature.

Calculation of maximal bound FhuA virus to the cantilever

Input parameters are in *italic.* Note that these calculations are rough estimations and ignore the spherical nature of the proteoliposomes significantly enlarging the active sensor surface.

Number of FhuA receptors on cantilever		
	Value	**Unit**
Coverage of cantilever with FhuA patches	*64%*	
Unit cell axis a	*12.4*	*nm*
Unit cell axis b	*9.8*	*nm*
Number of FhuA molecules per unit cells	*4*	
Symmetry related accessibility ($p22_12_1$)	*0.5*	
Cantilever width	100	µm
Cantilever length	500	µm
Area of cantilever	50000	μm^2

© 2009 **Macmillan Publishers Limited. All rights reserved.**

Area per FhuA molecule	0.00003038	μm^2
Minimal number of FhuA molecules on cantilever	1.1E+9	molecules
Minimal number of accessible FhuA on cantilever	5.3E+08	molecules

Table Suppl. 1: Structural information from Lambert et al. [4]. $P22_12_1$ symmetry assumed, or densely packed vesicle: Therefore only every second FhuA molecule will be accessible. This does not take double layers (vesicles) into account and ignores the spherical nature of the used proteoliposomes.

Number of T5 heads on cantilever		
	Value	**Unit**
Head size of phage	*~75*	nm
Unit cell of hexagonal arrangement	*14614.2*	*nm^2*
Number per unit cell	*2*	*phages*
Cantilever width	*100*	µm
Cantilever length	*500*	µm
Coverage of cantilever with FhuA patches	64	%
Number of densely packed phage heads on the cantilever *(if unspecifically physisorbed)*	6.84E+06	phages
Number of densely packed phage heads on FhuA functionalized cantilever areas	4.38E+06	phages

Table Suppl. 2: Estimation of maximal phage bound to the cantilever due to the head size of the T5-virus. Unspecific binding and hexagonal packing of the head is assumed.

Comparison with experiment		
	Value	**Unit**
Measured mass	*~8*	ng
Mass per phage	*7.0E+07*	*Da*
Mass per phage	*1.2 E-07*	*ng*
Number of measured phages	*6.7 E+07*	phages
Phage head packing ratio (measured specifically bound / calculated for unspecific adsorption)	*15*	
Percentage of occupied FhuA receptors	*13%*	occupation rate

© 2009 **Macmillan Publishers Limited. All rights reserved.**

Table Suppl 3: Phage mass calculations using the reported mass of Freifelder et al. (1970) [20]. *Phage head packing ratio:* Number of densely packed heads on the cantilever divided by the measured head phage number. *Percentage of occupied FhuA receptor:* FhuA Molecules with bound phages relative to the total amount of FhuA receptors.

References

1. Boulanger, P. et al. Purification and structural and functional characterization of FhuA, a transporter of the Escherichia coli outer membrane. *Biochemistry* **35**, 14216-14224 (1996).
2. Hochuli, E., Dobeli, H. & Schacher, A. New metal chelate adsorbent selective for proteins and peptides containing neighbouring histidine residues. *J. Chromatogr.* **411**, 177-184 (1987).
3. Jap, B. et al. 2D Crystallization: From Art to Science. *Ultramicroscopy* **46**, 45-84 (1992).
4. Lambert, O. et al. An 8-A projected structure of FhuA, A "ligand-gated" channel of the Escherichia coli outer membrane. *J. Struct. Biol.* **126**, 145-155 (1999).
5. Hendrickson, H.E. & McCorquodale, D.J. Genetic and Physiological Studies of Bacteriophage T5 I. An Expanded Genetic Map of T5. *J. Virol.* **7**, 612-618 (1971).
6. Braun, T. et al. Micromechanical mass sensors for biomolecular detection in a physiological environment. *Phys. Rev. E* **72**, 031907 (2005).
7. Braun, T. et al. Digital Processing of Multi-Mode Nano-Mechanical Cantilever Data. *J. Phys. Conf. Series* **61**, 341-345 (2007).
8. Braun, T. et al. Processing of kinetic microarray signals. *Sens. Act. B* **128**, 75-82 (2007).
9. Young, D. & Felgar Tables of Characteristic Functions Representing Normal Modes of Vibration of a Beam. *The University of Texas Publication* **44**, 1-32 (1949).
10. Braun, T., Kaufmann, T., Remigy, H. & Engel, A. in Encyclopedic Reference of Genomics and Proteomics in Molecular Medicine. (ed. D.R. Ganten, Klaus)2005).
11. Faraldo-Gomez, J.D. & Sansom, M.S.P. Acquisition of siderophores in Gram-negative bacteria. *Nature Rev. Mol. Cell Biol.* **4**, 105-116 (2003).
12. Locher, K.P. & Rosenbusch, J.P. Oligomeric states and siderophore binding of the ligand-gated FhuA protein that forms channels across Escherichia coli outer membranes. *Eur. J. Biochem.* **247**, 770-775 (1997).
13. Alves, I.D., Park, C.K. & Hruby, V.J. Plasmon resonance methods in GPCR signaling and other membrane events. *Curr. Protein Pept. Sci.* **6**, 293-312 (2005).
14. Zilberman, G. & Smith, A.L. QCM/HCC as a platform for detecting the binding of warfarin to an immobilized film of human serum albumin. *Analyst* **130**, 1483-1489 (2005).
15. Zhang et al. Rapid and label-free nanomechanical detection of biomarker transcripts in human RNA. *Nature Nanotech.* **1**, 214-220 (2006).
16. Backmann, N. et al. A label-free immunosensor array using single-chain antibody fragments. *Proc. Natl. Acad. Sci. USA* **102**, 14587-14592 (2005).
17. Braun, T. et al. Conformational change of bacteriorhodopsin quantitatively monitored by microcantilever sensors. *Biophys. J.* **90**, 2970-2977 (2006).
18. Pignon, F. et al. Structure and rheological behavior of casein micelle suspensions during ultrafiltration process. *J. Chem. Phys.* **121**, 8138-8146 (2004).
19. Gebhardt, R., Doster, W., Friedrich, J. & Kulozik, U. Size distribution of pressure-decomposed casein micelles studied by dynamic light scattering and AFM. *Eur. Biophys. J.* **35**, 503-509 (2006).
20. Freifelder, D. Molecular weights of coliphages and coliphage DNA. IV. Molecular weights of DNA from bacteriophages T4, T5 and T7 and the general problem of determination of M. *J. Mol. Biol.* **54**, 567-577 (1970).

© 2009 **Macmillan Publishers Limited. All rights reserved.**